Materials and Design 36 (2012) 671–678

Contents lists available at SciVerse ScienceDirect

Materials and Design

journal homepage: www.elsevier.com/locate/matdes

A constitutive description of the thermo-viscoplastic behavior of body-centered cubic metals

C.Y. Gao [a,b], W.R. Lu [a], L.C. Zhang [b,*], H.X. Yan [a]

[a] Department of Mechanics, Zhejiang University, Hangzhou 310027, China
[b] School of Mechanical and Manufacturing Engineering, The University of New South Wales, NSW 2052, Australia

ARTICLE INFO

Article history:
Received 15 September 2011
Accepted 6 December 2011
Available online 14 December 2011

Keywords:
E. Mechanical
F. Constitution
F. Plastic behavior

ABSTRACT

The Johnson–Cook (J–C) equation, which is obtained from the phenomenological observations of experimental data at relatively low strain rates, cannot well describe the dynamic thermo-mechanical response of many materials at high strain rates, especially under the situations of high or low temperatures. This paper develops a new physics-based model for the constitutive description of BCC metals through a thermal activation analysis of the dislocation motion in the plastic deformation of crystalline materials with the use of the mechanical threshold stress (MTS) as an internal state variable. It was found that the new model can effectively reflect the plastic deformation mechanism of BCC crystals because it directly relates the macroscopic state variables in the constitutive model with the micromechanical characteristics of materials. The material parameters of the model are efficiently determined by an optimization method to guarantee that the material parameters are globally optimal in their theoretically allowed ranges. The application of the model to HSLA-65 steel and Tantalum shows that it is much easier to apply than the MTS model, that its flow stress predictions are better than the Rusinek and Klepaczko (R–K), Abed, Zerilli and Armstrong (Z–A) and J–C models, and that the present model predictions are in good agreement with the experimental data in a broad range of strain rate, temperature and strain.

1. Introduction

High-strength low-alloy (HSLA) steels are a kind of important industrial materials and have been widely used in engineering structures. Compare with carbon steels, they have a carbon content lower than 0.25% and contain a low content of alloying elements, generally below 2.5%, but possess many superior mechanical properties such as high yield strength and strength-to-weight ratio (usually 20–30% lighter than carbon steels with the same strength), better formability and weldability, less possibility of low-temperature brittleness, lower notch and aging sensitivity, and greater resistance to corrosion from air and seawater. Due to their good properties above, HSLA steels have been extensively used in heavy machinery, mining equipment, ocean drilling platforms and large marines etc. In reality, the production of HSLA steels has occupied about ten percent of the steel production in advanced industrial countries.

An accurate description of the dynamic thermo-mechanical response of materials to high strain rate, elevated temperature and large strain is important in key engineering applications and materials design. Over the past decades, the investigation into the rate-dependent constitutive models has been extensive, among which the Johnson–Cook (J–C) equation, which is based on the conventional phenomenological theory, has been the most widely used [1]. However, it has been reported that the J–C model does not function well when a material is subjected to deformation at a very high strain rate, particularly at elevated temperature, such as in the cases of high speed machining (HSM), perforation, and crashing etc. [2]. Although some modified J–C models [3] and many other phenomenological models [4–6] were proposed to improve the constitutive descriptions of the dynamic plasticity of metals, these conventional models lack the necessary physical foundations in themselves, and the physically based models have been developed to overcome the difficulties and have received increasing attention, as introduced below.

Zerilli and Armstrong [7] proposed a dislocation-based Z–A constitutive relation with a thermal activation analysis of dislocation motion and rate-controlling mechanism of plastic deformation. They concluded that different crystalline structures (FCC, BCC and HCP) have different constitutive behaviors. Nemat-Nasser et al. developed a physical constitutive model applicable to both FCC and BCC metals [8–10]. Abed [11] proposed a constitutive relation to describe the plastic behavior of ferritic steels (e.g. HSLA-65 and DH-63), and pointed out that the yield stress is mainly captured by the thermal component of the flow stress while the strain hardening are totally pertained to the athermal component of the

* Corresponding author. Tel.: +61 2 9385 6078; fax: +61 2 9385 7316.
E-mail address: Liangchi.Zhang@unsw.edu.au (L.C. Zhang).

0261-3069/$ - see front matter © 2011 Elsevier Ltd. All rights reserved.
doi:10.1016/j.matdes.2011.12.012

flow stress. Rusinek et al. made an analysis for the thermo-viscoplastic behaviors of six high strength steels with a Rusinek–Klepaczko (R–K) model [12], and proposed a modified R–K model specially for FCC metals [13] and an extended R–K model for phase transformation phenomena [14]. Anurag and Guo [15] presented a modified micromechanical approach to determine the flow stress of work materials experiencing complex deformation histories in manufacturing processes. Balokhonov et al. [16] carried out 2D simulations of thermomechanical response of HSLA-65 steel at different strain rates and temperatures by using a physically based model developed from the Nemat-Nasser–Guo model [10]. A constitutive equation was developed in a different way based on dimensional analysis of the flow behavior for plain carbon steels [17]. Apart from the above, the constitutive models and related experimental results for metals and alloys in hot working reported in recent years have been critically reviewed in [18].

This paper will develop a new physical constitutive model for BCC metals based on the theory of thermal activation of dislocation motion. An optimization method developed previously by the authors [19] will be used to determine the constitutive parameters. To explore the applicability of the new model, the dynamic thermo-viscoplastic behavior of typical BCC metals, HSLA-65 steel as well as polycrystalline Tantalum, will be investigated.

2. Physics-based constitutive modeling

The physical constitutive modeling of BCC metals is mainly based on the theory of thermally activated dislocation kinetics. In the thermal activation analysis, plasticity is produced by the motion of defects (dislocations) at all temperatures which has to overcome the obstruction of short-range and long-range barriers. The short-range barriers include forest dislocations (i.e., the intersection of dislocation forests in FCC metals), Peierls stress (i.e., the critical shear stress required to overcome Peierls barriers to move a dislocation in BCC metals), point defects (e.g., vacancies and self-interstitials), alloy elements, solute atoms (interstitials and substitutionals), impurities, deposits and so on. The long-range barriers include grain boundaries, far-field dislocation forests and other microstructural elements with far-field influence. The former is mainly overcome by thermal activation while the latter is basically independent of the temperature (i.e., athermal). Therefore, the flow stress (σ), which is essentially defined by the material resistance to dislocation motion, can be decomposed into $\sigma = \sigma_{ath} + \sigma_{th}$. Where σ_{th} is the thermal component of the flow stress reflecting the effect of the short-range barriers closely related to the thermal activation, and σ_{ath} is the athermal component of the flow stress reflecting the effect of the long-range barriers.

At the same time, the mechanical threshold stress (MTS) defined as the flow stress at 0 K was proposed by Follansbee and Kocks [20] in the constitutive modeling. It can be similarly decomposed into $\hat{\sigma} = \hat{\sigma}_{ath} + \hat{\sigma}_{th}$. Where $\hat{\sigma}$ denotes the MTS, $\hat{\sigma}_{ath}$ and $\hat{\sigma}_{th}$ are the athermal and thermal components of $\hat{\sigma}$. At absolute zero degree, there is no thermal activation energy, so the height of the short-range barriers is maximal. When temperature increases, the height will fall due to the increase of the vibration amplitude of the atoms activated by the thermal energy, making a dislocation easier to overcome the barriers. Thus the thermal stress component of the flow stress decreases with the rise of temperature while the athermal stress remains unchanged. By using the MTS as a reference stress that characterizes the constant structure of a material, the flow stress can be expressed as:

$$\sigma = \sigma_{ath} + \sigma_{th} = \hat{\sigma}_{ath} + f(\dot{\varepsilon}, T) \cdot \hat{\sigma}_{th} \tag{1}$$

where $\dot{\varepsilon}$ (plastic strain rate) and T (absolute temperature) are the state variables, $f(\dot{\varepsilon}, T)$ is the thermal activation function (<1) representing the influence of strain rate hardening and temperature softening. The structural evolution will be involved in the part of $\hat{\sigma}_{th}$. Now, the three internal state variables in Eq. (1), $\hat{\sigma}_{ath}$, f and $\hat{\sigma}_{th}$, will be determined respectively.

2.1. Athermal stress $\hat{\sigma}_{ath}$

It has known that there exists an important difference between BCC and FCC metals in their dislocation motion mechanisms due to their different crystalline structures. The thermal activation area is closely related with strain for FCC metals but not for BCC metals. In other words, the strain hardening of BCC metals is not coupled in the thermal stress but belongs to the athermal stress. Hence, if the strain hardening of BCC metals follows a power-law form [7], the athermal stress will be

$$\hat{\sigma}_{ath} = (\sigma_G + \tilde{k} d^{-1/2}) + K\varepsilon^n \tag{2}$$

where ε is plastic strain, K is strain hardening coefficient, n is strain hardening exponent; σ_G is the stress due to initial defects or impurities, d is the diameter of the grain and $\tilde{k}$ is the microstructural stress modulus. The term, $\tilde{k} d^{-1/2}$, following the classic Hall–Petch relationship, stands for the size effect of grain on flow stress [21]. The size effect can be regarded as a constant for a given material if there is no obvious physical change to alter the average grain size during plastic deformation.

2.2. Thermal activation function f

Based on the Arrhenius expression deduced from the relations of Orowan [22] and Johnson and Gilman [23], and the expression of Gibbs free energy proposed firstly by Kocks et al. [24], the thermal activation function, f, at the current constant structure can be deduced as:

$$f(\dot{\varepsilon}, T) = \left\{ 1 - \left[-\frac{kT}{G_0} \ln\left(\frac{\dot{\varepsilon}}{\dot{\varepsilon}_0}\right) \right]^{1/q} \right\}^{1/p} \tag{3}$$

where k is the Boltzmann constant, $G_0 (= g_0 \mu b^3)$ is the reference free energy at 0 K (g_0 is nominal activation energy, μ is the shear modulus of material, b is the Burgers vector representing the excursion induced by dislocation), $\dot{\varepsilon}_0$ is the reference strain rate, p and q are a pair of parameters representing the shape of any potential barrier of crystals.

2.3. Thermal component of MTS $\hat{\sigma}_{th}$

The equation describing the saturated value of MTS, $\hat{\sigma}_s$, for FCC metals has been given in [20]. As discussed in [19], this saturation equation can be reasonably applied to BCC metals too, and has been used by Follansbee and Kocks in the constitutive description of 304L stainless steel [20] – a valid precedent of application to BCC metals. So, by using the saturation equation together with the decomposition form $\hat{\sigma}_s = \hat{\sigma}_{ath,s} + \hat{\sigma}_{th,s}$, there is

$$\hat{\sigma}_{th,s} = \hat{\sigma}_{s0} \exp\left[\left(\frac{kT}{g_{s0}\mu b^3} \right) \ln\left(\frac{\dot{\varepsilon}}{\dot{\varepsilon}_{s0}} \right) \right] - \hat{\sigma}_{ath,s} \tag{4}$$

where $\hat{\sigma}_{s0}$ is the saturated reference value of $\hat{\sigma}$, $\dot{\varepsilon}_{s0}$ is the saturated reference value of strain rate, and g_{s0} is equivalent to the saturated value of g_0. All of them are constants and related with the microstructure of materials. Because the thermal stress of BCC metals is independent of straining, the saturated value of the thermal component of MTS should be the same as itself, i.e., $\hat{\sigma}_{th,s} = \hat{\sigma}_{th}$. Furthermore, the saturated value of the athermal component of MTS should be a constant if the athermal stress is independent of strain rate and temperature. Therefore

$$\hat{\sigma}_{th} = \hat{Y}\exp\left[\left(\frac{kT}{g_{s0}\mu b^3}\right)\ln\left(\frac{\dot{\varepsilon}}{\dot{\varepsilon}_{s0}}\right)\right] - \hat{S} \tag{5}$$

where $\hat{Y} = \hat{\sigma}_{s0}$ and $\hat{S} = \hat{\sigma}_{ath,s}$ are constants.

2.4. The complete constitutive relation

By substituting Eqs. (2), (3), and (5) into Eq. (1), the complete constitutive relation can be obtained:

$$\sigma = \sigma_0 + K\varepsilon^n + \left\{\hat{Y}\exp\left[\alpha T\ln\left(\frac{\dot{\varepsilon}}{\dot{\varepsilon}_{s0}}\right)\right] - \hat{S}\right\} \cdot \left\{1 - \left[-\beta T\ln\left(\frac{\dot{\varepsilon}}{\dot{\varepsilon}_0}\right)\right]^{1/q}\right\}^{1/p} \tag{6}$$

where $\sigma_0 = (\sigma_G + \tilde{k}d^{-1/2})$, $\alpha = k/(g_{s0}\mu b^3)$ and $\beta = k/(g_0\mu b^3)$.

The material parameters in this constitutive relation are $(\sigma_0, K, n, \hat{Y}, \hat{S}, \alpha, \beta, \dot{\varepsilon}_{s0}, \dot{\varepsilon}_0, p, q)$. This one-dimensional constitutive equation can be extended to 3D descriptions by relating the true stress and plastic strain with the Mises equivalent stress and equivalent plastic strain. The isotropy is assumed for the macroscopic material behavior and the J_2 theory is applied in 3D generalization [25]. The 3D constitutive relation can then be implemented into a finite element code for applications. A framework of an explicit integration algorithm of the thermo-viscoplastic constitutive relation compatible with finite element codes has been presented in [26]. An implicit integration scheme has also been demonstrated [27].

The following understanding is useful in the application of the above constitutive relation.

2.4.1. Adiabatic shear phenomenon

The constitutive relation is applicable not only to an isothermal deformation process but also to an adiabatic deformation process (which mainly happens at relatively high strain rates $>10^2\ s^{-1}$ and at temperature below $0.4T_m$). If a localized adiabatic shear band (ASB) occurs, the majority of the plastic work will be converted to the internal dissipation heat causing a local rapid increase of temperature in materials (there is an empirical converting coefficient, essentially 1.0 for large strains beyond 20% [10]). The plastic work, $W^P = \int_0^{\varepsilon}\sigma(\varepsilon,\dot{\varepsilon},T)d\varepsilon$, can be incrementally integrated by using the mean-value theorem for the integration in each strain increment [8]. Then the rise of temperature calculated from the above energy conversion relationship will depend on the density of the material (ρ), the specific heat of the material at a constant pressure (c_p) and the magnitude of plastic work. In the adiabatic calculation of flow stress by the constitutive relation of Eq. (6), the state variable of temperature must be updated successively in each strain increment.

2.4.2. Critical temperature

During a plastic deformation process, the thermal activation in a material will decrease gradually with the rise of temperature and disappear eventually at a critical temperature. The formula of evaluating the critical temperature can be obtained by the condition that the thermal stress should not be negative [8]. So the critical temperature for the constitutive relation of Eq. (6) is $T^{cr} = [-\beta\ln(\dot{\varepsilon}/\dot{\varepsilon}_0)]^{-1}$. If temperature is beyond its critical value, the thermal component of flow stress should not be kept anymore. In this case, only the athermal stress remains.

2.4.3. Dynamic strain aging

It is common that the effect of dynamic strain aging (DSA) is related to the pinning of dislocations by diffusing solute atoms (in steel, mainly C and N) during the aging period. The mobility of solute atoms which diffuse to dislocations above a certain temperature produces additional resistance to dislocation motion, resulting in DSA when the dislocations are waiting at their short-range barriers. Nemat-Nasser and Guo pointed out, according to their experimental results, that slight DSA occurs in a temperature range of [400, 800] K at low strain rates ($>0.001\ s^{-1}$) and [600, 1000] K at high strain rates ($<3000\ s^{-1}$). This means that the temperature range of DSA shifts to higher temperatures when strain rates increase. Though Nemat-Nasser and Guo did not include the effect of DSA in their model, their model without DSA tallies well with the experimental results over a wide range of temperatures and strain rates. This indicates that the effect of DSA occurring within a certain local temperature range is limited and does not change the main tendency of the flow stress. Hence, in the present modeling the effect of DSA is not included too. Nevertheless, the way to consider the effect of DSA in the constitutive model can be found in [28,29].

2.4.4. Deformation twinning

Deformation twins always happen in the plastic deformation of BCC and HCP metals at high strain rates. As forementioned in this section, the twin effect can be incorporated in the athermal stress, and that the empirical power-law expression for the athermal stress is still suitable for twinning [19], provided that the material parameters in the athermal stress are determined correspondingly by the experimental data obtained in the case of twinning.

3. Determination of model parameters

HSLA-65 steel has a BCC structure in terms of its iron–carbon phase diagram. This advanced industrial steel is therefore used as an example. Its chemical composition and major mechanical properties are listed in Tables 1 and 2, respectively.

As the athermal stress is not coupled with the thermal stress and has the form of a simple power function, its parameters can be separately determined firstly. The experimental data used for the athermal stress should be at the high temperature where the flow stress is essentially independent of temperature [10]. The three parameters can be obtained just by power-function curve fitting:

$$\sigma_0 = 30\ \text{MPa}, K = 729\ \text{MPa}, n = 0.15$$

The two reference strain rates, $\dot{\varepsilon}_0$ and $\dot{\varepsilon}_{s0}$, can be assumably evaluated in advance. Since they are in the logarithmic functions, their influence is much smaller than α and β. Furthermore, as they are related with α and β, their evaluating errors can be offset in fitting α and β. This way not only avoid the largely scattered values of the two reference strain rates reported in the literature, but also enhance the calculation robustness of the multi-variables nonlinear optimization for the remaining six parameters. The typical value of the reference strain rate is known as $\dot{\varepsilon}_0 = 4\times10^8$ [10], and the probable value of the saturated reference strain rate can be evaluated as $\dot{\varepsilon}_{s0} = 4\times10^{10}$ considering that it is generally greater than $\dot{\varepsilon}_0$ by two orders.

With the above parameters ready, the remaining six parameters, $(\hat{Y}, \hat{S}, \alpha, \beta, p, q)$, can be determined as a whole by a mixed multi-variables nonlinear optimization method. The new optimization method which combines a local algorithm (LA) with a global algorithm (GA) has been introduced by the authors in [19]. A Matlab program has been developed to carry out the optimization calculations. And the experimental results of the flow stress–strain curves of HSLA-65 steel at $3000\ s^{-1}$ [10] are used as the data of benchmark. In addition, these parameters' ranges need to be determined as the constraints of the optimization algorithm, so it is necessary to evaluate the physically available ranges of these material

Table 1
Major alloy content of HSLA-65 steel (wt.%).

C	Mn	Cu	Si	Cr	Mo	V	Ti	Al	Nb	Ni	P	S	Balance
0.08	1.40	<0.01	0.24	0.01	0.02	0.07	0.01	0.03	0.04	<0.01	0.005	0.005	Fe

Table 2
Principal mechanical properties of HSLA-65 steel.

Yield strength (MPa)	Tensile strength (MPa)	Shear modulus (GPa)	Young's modulus (GPa)	Poisson's ratio	Elongation percentage (%)	
					200 mm gauge length	50 mm gauge length
448	537–689	80	210	0.3	18	22

parameters to guarantee the rationality of optimized results. The evaluations are given below.

3.1. Ranges of $\hat{Y}$ and $\hat{S}$

Since it is generally assumed that strain hardening arrives at the saturation state when the strain is equal to about 1.0, the median value of $\hat{S}$ can be known as $\hat{S} = \hat{\sigma}_{ath,s}|_{\varepsilon=1} = 758$ MPa. The probable range of $\hat{S}$ is evaluated as [700, 800] MPa to cover the possible variation of the saturated strain. In addition, the term $\{\hat{Y}\exp[\alpha T \ln(\dot{\varepsilon}/\dot{\varepsilon}_{s0})] - \hat{S}\}$ in the thermal stress is equivalent to the parameter $\hat{\tau}$ (=1450 MPa) in the Nemat-Nasser–Guo model [10]. Based on this relationship, the range of $\hat{Y}$ can be evaluated as [2156, 3807] MPa and slightly extended to [2000, 4000] MPa.

3.2. Ranges of α and β

In the definition of $\beta = k/(g_0\mu b^3)$, the Boltzmann constant $k = 1.3806505 \times 10^{-23} J/K$, shear modulus $\mu = 80$ GPa and Burgers vector $b = 3.3 \times 10^{-10} m$ are known. The only unknown constant is the nominal activation energy g_0. However, it is known that g_0 is within the range of [0.2, 2] for medium strength of a single obstacle of barriers [30]. Thus the range of β may be evaluated as $[2.4 \times 10^{-6}, 2.4 \times 10^{-5}]$. Since there is $\beta = k/G_0 = 1.06 \times 10^{-4}$ in [6], its range can be extended to $[2.4 \times 10^{-6}, 2.4 \times 10^{-4}]$ to cover a wider span of g_0. For $\alpha = k/(g_{s0}\mu b^3)$, its range can be the same as β because g_{s0} has the similar order as g_0.

3.3. Ranges of p and q

It is known that (p, q) is a pair of parameters representing the shape of the crystal potential barrier. According to the physical nature of the barrier, there are $p \in (0, 1]$ and $q \in [1, 2]$ for a single crystal structure. The value of (2/3, 1) for (p, q) means a rectangular barrier, (1/2, 2) is a hyperbolic barrier and (1, 2) is a sinusoidal barrier. For commonly used metals, some other typical values such as (2/3, 2), (3/4, 4/3) and (1, 1) can all be considered as the transitional shape between the rectangle and the sinusoid.

After determined these parameter ranges, a mixed multi-variables nonlinear optimization were carried out and a group of optimal constitutive parameters were obtained for HSLA-65 steel, as listed in Table 3.

Table 3
Final optimal results of constitutive parameters for HSLA-65 steel.

Constitutive parameters	Theoretically allowed range	Optimal results	Unit
$\hat{Y}$	[2000, 4000]	2007	MPa
$\hat{S}$	[700, 800]	712	MPa
α	$(2.4 \times 10^{-6}, 2.4 \times 10^{-4})$	5.97×10^{-6}	$1/K$
β	$(2.4 \times 10^{-6}, 2.4 \times 10^{-4})$	1.08×10^{-4}	$1/K$
p	[0, 1]	2/3	/
q	[1, 2]	2	/

4. Results and discussions

The predictions for HSLA-65 steel by the new model developed above are compared with those of some other physical constitutive models including the Abed model, the R–K model, the Nemat-Nasser and Guo (P–B) model, and the phenomenological J–C model (where the material constants for the J–C model calculations are $A = 790$ MPa, $B = 1320$ MPa, $n = 0.25$, $C = 0.022$, $m = 0.35$). It should be noted that the material parameters of these models are all determined by the same set of experimental data [10]. The conclusion from such a comparison will therefore make sense in terms of the applicability of the new model. In addition, all the flow stress predictions in the following figures correspond to the adiabatic deformation process except the quasi-static loading ($0.001\ s^{-1}$) case and the specially presented isothermal case.

The flow stress predictions of the proposed model and the other models mentioned above for HSLA-65 steel are compared at $3000\ s^{-1}$ and different initial temperatures in Fig. 1, based on the experimental results of Nemat-Nasser and Guo [10]. At room temperature these models are basically conformable with each other and agree well with the experimental data. At low or high temperatures, however, the J–C model and R–K model bifurcate away from the flow stress, and the Abed model's predictions are higher than the experimental data. It is clear that the proposed model is satisfactory in the whole temperature range. This means that the new model has essentially captured the main mechanism of the temperature effect of the material.

It is noticed in Fig. 1 that the strain hardening rates in these stress–strain curves at different temperatures are obviously different. The reason for this is actually the result of competition between the strain hardening effect and the thermal softening effect [31]. At room temperature, the stress–strain curve becomes almost flat when the strain exceeds a certain value, indicating that strain hardening and thermal softening basically arrive at a balance state. At a low temperature, the thermal softening effect due to adiabatic shear becomes exponentially increscent and exceeds strain hardening, but at a high temperature it is very limited and lower than strain hardening. Since the thermal softening effect increases with the plastic strain, the starting point of the 'flat' stress–strain curve does not mean the beginning of the saturation state. Actually, the saturation of strain hardening of HSLA-65 steel happens relatively lately at quite a large strain. Here saturation means that the strain hardening rate finally decreases to zero and the flow stress reaches an invariant saturated value when beyond a critical plastic strain. It is resulted from the dynamic recov-

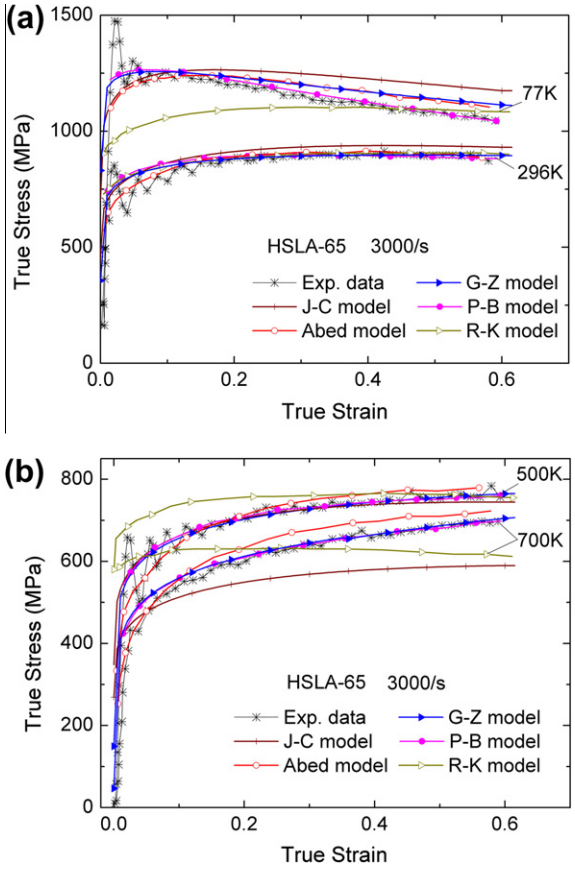

Fig. 1. Comparison of the flow stress predictions of the present model and other models for HSLA-65 steel based on the experimental data [10] at 3000 s^{-1} and different initial temperatures: (a) 77 K and 296 K, and (b) 500 K and 700 K.

ery of dislocations occurring by cross slip, an important role in the thermally activated process of BCC metals [32].

In addition, the power-law expression has generally been used as an approximate description of strain hardening in the athermal components of the flow stress in BCC metals [7], but it cannot describe the saturation of strain hardening in itself. So the strain hardening effect may be over-evaluated especially when close to the saturation. However, there is not a noticeable error in the general strain range (below 1.0) by using the power-law expression for BCC metals. An exponential expression [11], which has an asymptote in the function itself, is capable of describing the saturation of strain hardening.

The isotherms of different models of HSLA-65 steel are compared with the experimental results at a strain rate of 3000 s^{-1} and room temperatures in Fig. 2. It can be seen again that the proposed model is still better than the P–B and J–C models in the isothermal case. At the same time, the adiabatic curve of the present model is also presented for comparison. The difference between the adiabat and isotherm can quantitatively reflect the effect of adiabatic shear phenomenon on the flow stress. Besides, the experimental sample in Fig. 2 was interruptedly tested by incremental loadings [10] so as to show the repeatability and consistency of SHPB measurement, which finally proves the reliability of the experimental data used here.

Fig. 3 compares the flow stress predictions of different models for HSLA-65 steel at 8500 s^{-1} and indicated initial temperatures. Obviously, the proposed model can well describe the flow stress at a quite high strain rate (close to 10^4 s^{-1}), while the J–C model cannot correctly reflect the dependence of the flow stress on temperature, especially at the high side. Note that the experimental

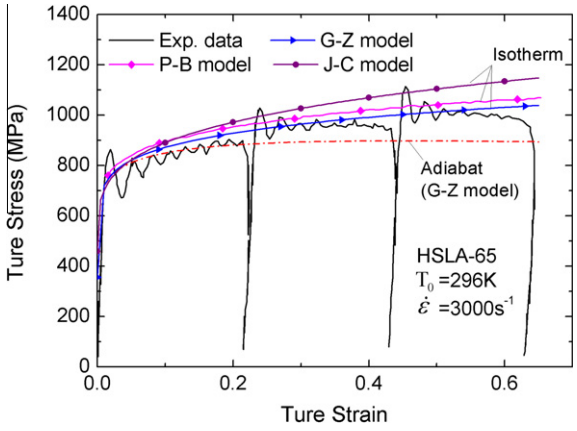

Fig. 2. Comparison of isothermal stress–strain relations predicted by different models of HSLA-65 steel with experimental results [10] at a strain rate of 3000 s^{-1} and room temperatures.

results at such a high strain rate could be unstable and occur more fluctuation due to the technological difficulties encountered in the measurement even by using a set of enhanced SHPB apparatus as introduced in [9]. This may be the reason for the inharmonic deviation occurring in the prediction curve of the present model at 500 K. Fig. 4 presents the flow stress predictions of different models under quasi-static loading of 0.001 s^{-1}. In the case of very low strain rates, the predictions of all models, except the J–C model, are in good agreement with the experimental results. The J–C

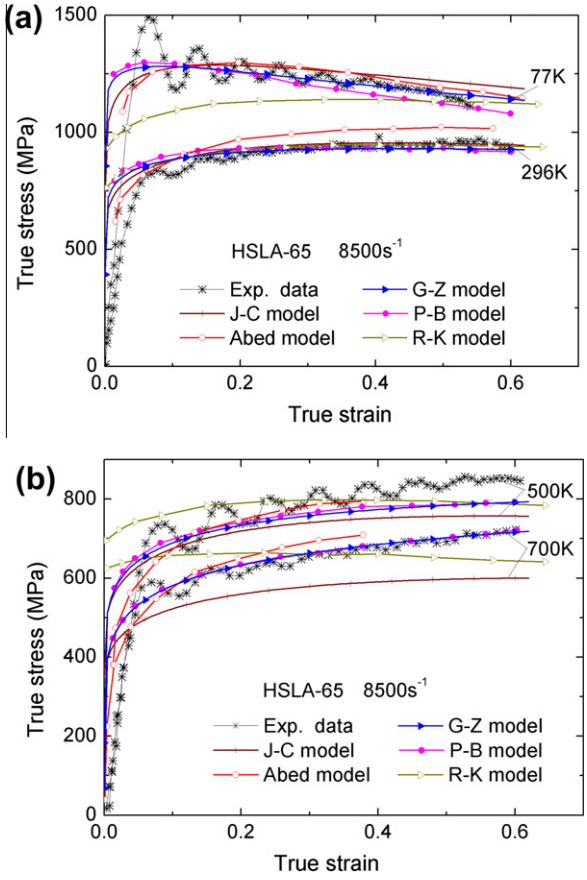

Fig. 3. Comparison of the flow stress predictions of the present model and other models for HSLA-65 steel based on the experimental data [10] at 8500 s^{-1} and different initial temperatures: (a) 77 K and 296 K, and (b) 500 K and 700 K.

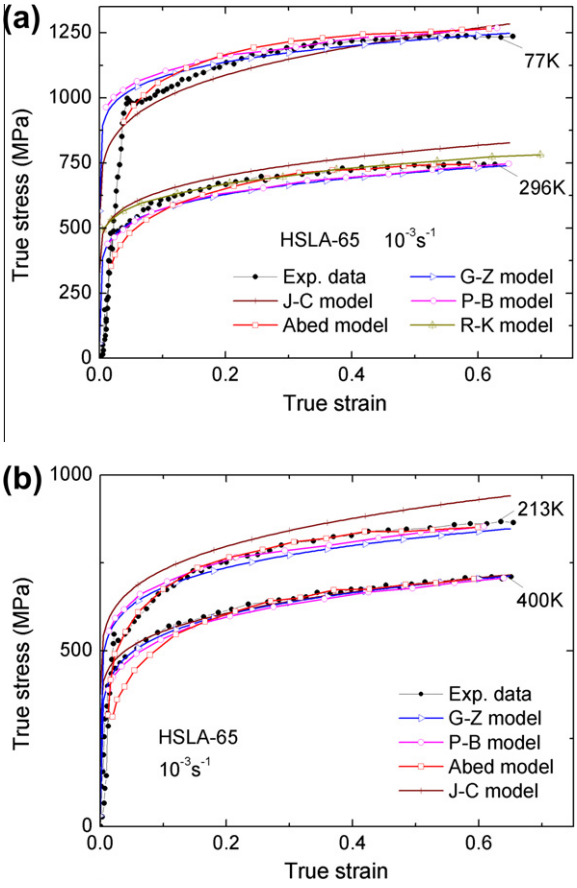

Fig. 4. Comparison of the flow stress predictions of the present model and other models for HSLA-65 steel based on the experimental data [10] at 0.001 s^{-1} and different initial temperatures: (a) 77 K and 296 K, and (b) 213 K and 400 K.

model seems to be applicable at low and high temperatures at this time, but gives an error of 15% in the room temperature range.

The dependence of the flow stress on temperature for HSLA-65 steel at the strain of 15% and three different strain rates is shown in Fig. 5. It is seen that the proposed model gives a good description of the dependence of the flow stress on temperature for the material dynamic response, while the Abed model appears increasing deviation from the room temperature to low temperature at high strain rates. All the flow stress curves decay with temperature and approach to their minimum values when the temperature is close to the so-called critical temperature (to be illustrated specially in the next figure). In other words, the thermal component of the flow stress approaches zero at the critical temperature, and only the athermal stress remains as a constant relative to temperature. This confirms that it is rational to decompose the flow stress into the athermal and thermal components during the constitutive modeling. Furthermore, the flow stress of HSLA-65 steel decreases rapidly with temperature especially at low temperature but slowly when beyond room temperature at 0.001 s^{-1} (or below 0.1 s^{-1}), which reveals that this material has a good weldability since its strength is not temperature-sensitive at high temperature [10]. In addition, it is also noticed that at the strain rate of 0.001 s^{-1}, the experimental data gradually rise within the temperature range 400–600 K, which may result from the beginning of the DSA effect that has been neglected in the present model.

Fig. 6 presents the dependence of critical temperature on strain rate predicted by the proposed model and the Abed model for HSLA-65 steel, based on the related discussion about critical temperature in Section 2. For the stain rates of 0.001 s^{-1}, 3000 s^{-1}

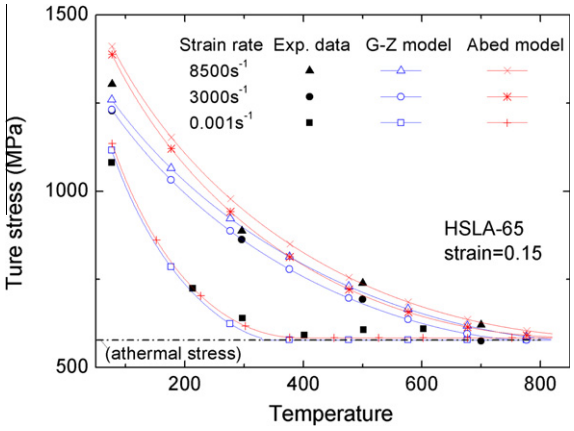

Fig. 5. Dependence of the flow stress on temperature for HSLA-65 steel, predicted by the present model and the Abed model compared to the experimental results at 15% strain and indicated different strain rates.

and 8500 s^{-1}, the critical temperatures predicted by the proposed model are 331, 746, and 819 K, respectively. It can be seen from this figure that the critical temperature predicted by the Abed model is higher due to the different values of model parameters determined individually. The physical explanation about the critical temperature, can be as follows. There is no thermal activation energy at 0 K, so the height of the short-range barriers to dislocations is maximal. When temperature increases, the height will fall due to the increase of the atom vibration amplitude activated by the thermal energy, which helps a dislocation to overcome the Peierls-Nabarro barriers in BCC metals or the forest-dislocation barriers in FCC metals [31]. Thus, the thermal stress which reflects the effect of the short-range barriers will decrease with the increasing temperature, and will disappear finally when the short-range barriers cease to function. So there must be a critical temperature introduced to avoid appearing a minus value of thermal stress in the constitutive relation.

The relations of the flow stress and strain rate for HSLA-65 steel at 15% strain and different temperatures are revealed in Fig. 7. The predictions of the proposed model are quite consistent with the experimental results while the Abed model's predictions are somewhat high especially at the low temperature end. Kocks and Follanssbee [20] have pointed out, based on their experimental results of pure copper, that in FCC metals there exist a remarkable

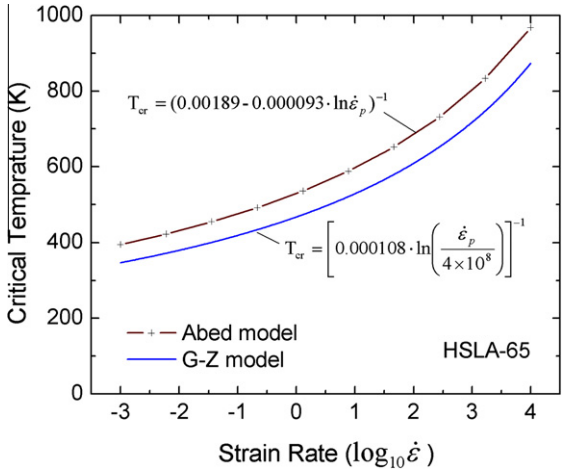

Fig. 6. Critical temperatures predicted by the present model and the Abed model for HSLA-65 steel at various strain rates.

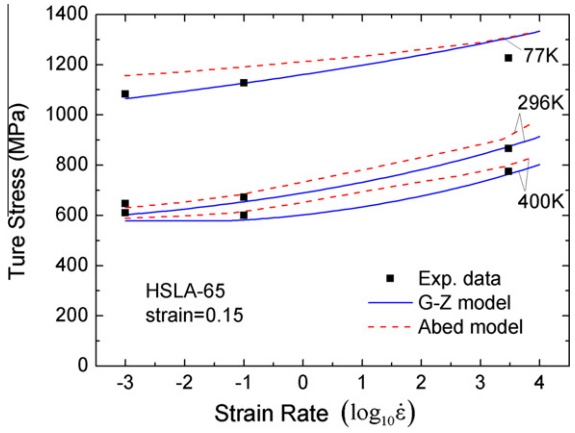

Fig. 7. Relation of the flow stress and strain rate for HSLA-65 steel, predicted by the present model and the Abed model compared to the experimental results at 15% strain and indicated different temperatures.

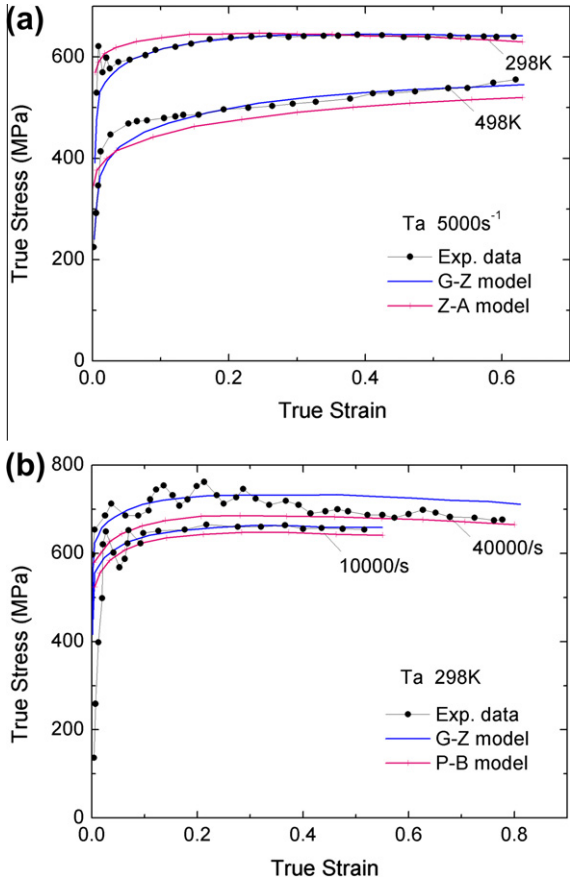

Fig. 8. Flow stress predictions of the present model and other models for Tantalum based on the experimental data [8] at: (a) 5000 s^{-1} and 298, 498 K, and (b) very high strain rates and room temperature.

upturn phenomenon in the relation of flow stress and strain rate because of the rapid increase of the rate sensitivity of flow stress when the strain rate approaches or exceeds 10^4 s^{-1}. But in BCC metals, it seems that there is no such phenomenon as shown in Fig. 7, which is an important difference between the high-strain-rate responses of BCC and FCC metals. This implies that the applicable strain rate range of the present model for BCC metals can be rationally extended to beyond 10^4 s^{-1} without model correction [8].

The flow stress predictions of the proposed model and other models for polycrystalline Tantalum are provided in Fig. 8, to show that the proposed model is applicable not only to ferrous alloy steels but also to nonferrous BCC metals. The model predictions are compared with experimental data [8] at high temperature ($\sim$ 498 K) in Fig. 8a and at very high strain rates ($1 \times 10^4\ s^{-1} - 4 \times 10^4\ s^{-1}$) in Fig. 8b. The results indicated that it should be reliable to apply the new model proposed in this paper to most BCC metals and alloys.

5. Conclusions

Based on the thermal activation analysis of the dislocation motion in the plastic deformation of BCC metals, a new physics-based constitutive model for BCC metals has been developed. The new model with globally-optimized material parameters well describes the effects of temperature and strain rate, and rationally reflects the influence of structural evolution on the flow stress. It is simpler and easier to use than the original MTS model, and gives better predictions than the R–K, Abed, Z–A and J–C models, in terms of the thermo-mechanical viscoplastic behavior of HSLA-65 structural steel and Tantalum, based on the experimental results in a broad range of strain rate, temperature and strain. In addition, the new model can be implemented as a dynamic/quasi-static yield surface into the stress updating formulation in finite element simulations of large plastic deformation of BCC materials. Compared with the mostly used J–C model in general finite element software, it can describe more accurately the dynamic plasticity of BCC metals, especially at a high or low temperature.

Acknowledgements

This research work was supported by the Australian Research Council and the National Natural Science Foundation of China (No. 50877070) together with the Open Foundation of State Key Laboratory of Explosion Science and Technology of China (No. KFJJ11-9Y).

References

[1] Johnson G, Cook W. Fracture characteristics of three metals subjected to various strain, strain rates, temperature and pressures. Eng Fract Mech 1985;21:31–48.
[2] Arsecularatne JA, Zhang LC. Assessment of constitutive equations used in machining. Key Eng Mater 2004;274:277–82.
[3] Yu HD, Guo YJ, Lai XM. Rate-dependent behavior and constitutive model of DP600 steel at strain rate from 1E–4 to 1E+3 s^{-1}. Mater Des 2009;30:2501–5.
[4] Khan AS, Huang S. Experimental and theoretical study of mechanical behavior of 1100 aluminum in the strain rate range 1E–5 1E4/s. Int J Plast 1992;8:397–424.
[5] Cai J, Li FG, Liu TY, Chen B, He M. Constitutive equations for elevated temperature flow stress of Ti–6Al–4V alloy considering the effect of strain. Mater Des 2011;32:1144–51.
[6] Durrenberger L, Molinnari A. Modelling of temperature and strain-rate effects in metals using an internal variable model. Exp Mech 2009;49:247–55.
[7] Zerilli FZ, Armstrong RW. Dislocation-mechanics-based constitutive relations for material dynamics calculation. J Appl Phys 1987;5:1816–25.
[8] Nemat-Nasser S, Isaacs JB. Direct measurement of isothermal flow stress of metals at elevated temperatures and high strain rates with application to Ta and Ta-W alloys. Acta Mater 1997;45:907–19.
[9] Nemat-Nasser S, Li YL. Flow stress of FCC polycrystals with application to OFHC Cu. Acta Mater 1998;46:565–77.
[10] Nemat-Nasser S, Guo WG. Thermomechanical response of HSLA-65 steel plates: experiments and modelling. Mech Mater 2005;37:379–405.
[11] Abed FH. Constitutive modelling of the mechanical behavior of high strength ferritic steels for static and dynamic applications. Mech Time-Dependent Mater 2010;14:329–45.
[12] Rusinek A, Rodríguez-Martínez JA, Klepaczko JR, Pecherski RB. Analysis of thermo-visco-plastic behaviour of six high strength steels. Mater Des 2009;30:1748–61.
[13] Rusinek A, Rodríguez-Martínez JA, Arias A. A thermo-viscoplastic constitutive model for FCC metals with application to OFHC copper. Int J Mech Sci 2010;52:120–35.
[14] Rodríguez-Martínez JA, Rusinek A, Klepaczko JR, Pecherski RB. Extension of R–K constitutive relation to phase transformation phenomena. Mater Des 2009;30:2513–20.

[15] Anurag S, Guo YB. A modified micromechanical approach to determine flow stress of work materials experiencing complex deformation histories in manufacturing processes. Int J Mech Sci 2007;49:909–18.
[16] Balokhonov RR, Romanova VA, Schmauder S. Finite-element and finite-difference simulations of the mechanical behavior of austenitic steels at different strain rates and temperatures. Mech Mater 2009;41:1277–87.
[17] Phaniraj MP, Lahiri AK. Constitutive equation for elevated temperature flow behavior of plain carbon steels using dimensional analysis. Mater Des 2008;29:734–8.
[18] Lin YC, Chen XM. A critical review of experimental results and constitutive descriptions for metals and alloys in hot working. Mater Des 2011;32:1733–59.
[19] Gao CY, Zhang LC, Yan HX. A new constitutive model for HCP metals. Mater Sci Eng A 2011;528:4445–52.
[20] Follansbee PS, Kocks UF. A constitutive description of the deformation of copper based on the use of mechanical threshold stress as an internal state variable. Acta Metall 1988;36:81–93.
[21] Lederich RJ, Sastry SML, O'Neal JE, Rath BB. The effect of grain size on yield stress and work hardening of polycrystalline titanium at 295 K and 575 K. Mater Sci Eng A 1978;33:183–8.
[22] Orowan E. Problems of plastic gliding. Proc Phys Soc 1940;52:8–22.
[23] Johnson WG, Gilman JJ. Dislocation velocities, dislocation densities, and plastic flow in lithium fluoride crystals. J Appl Phys 1959;30:129–44.
[24] Kocks UF, Argon AS, Ashby MF. Thermodynamics and kinetics of slip. In: Progress in Materials Science, vol. 19. Oxford: Pergamon Press; 1975.
[25] Zaera R, Fernández-Sáez J. An implicit consistent algorithm for the integration of thermoviscoplastic constitutive equations in adiabatic conditions and finite deformations. Int J Solids Struct 2006;43:1594–612.
[26] Amirkhizi AV, Nemat-Nasser S. A framework for numerical integration of crystal elasto-plastic constitutive equations compatible with explicit finite element codes. Int J Plast 2007;23:1918–37.
[27] Rusinek A, Zaera R, Klepaczko JR. Constitutive relations in 3-D for a wide range of strain rates and temperatures – application to mild steels. Int J Solids Struct 2007;44:5611–34.
[28] Cheng JY, Nemat-Nasser S. A model for experimentally-observed high-strain-rate dynamic strain aging in titanium. Acta Mater 2000;48:3131–44.
[29] Rusinek A, Rodríguez-Martínez JA. Thermo-viscoplastic constitutive relation for aluminium alloys, modeling of negative strain rate sensitivity and viscous drag effects. Mater Des 2009;30:4377–90.
[30] Frost HJ, Ashby MF. Deformation mechanism maps. Oxford: Pergamon Press; 1982.
[31] Meyers MA. Dynamic behavior of materials. New York: John Wiley & Sons; 1994.
[32] Rhee M, Zbib H, Hirth JP, Huang H, Rubia T. Models for long-/short-range interactions and cross slip in 3D dislocation simulation of BCC single crystals. Model Simul Mater Sci Eng 1998;6:467–92.